



Multi-criteria comparative analysis of the pressure drop on coal gangue fly-ash slurry at different parts along an L-shaped pipeline

Defeng Wang¹ · Dengwu Jiao² · Zhanbo Cheng³ · Qingwen Shi⁴ · Helmut Mischo¹

Received: 9 August 2022 / Revised: 15 November 2022 / Accepted: 13 March 2023
© The Author(s) 2023

Abstract

Disposing of coal gangue and fly-ash on the surface is a risky method with tremendous potential catastrophic consequences for the environment. Backfill mining is a promising practice for turning those hazardous wastes into functional backfill materials. Unfortunately, how to efficiently deliver the slurry to the desired places remains under-researched. To address this issue, the computational fluid dynamics software Fluent was used in the current study in addition to a laboratory rheological test to simulate the impact of various parameters on the evolution of pressure at a particular section of the pipeline. Furthermore, the response surface method was employed to investigate how the various components and their corresponding influencing weights interact to affect the pressure drop. This study demonstrates that the pressure drop of the slurry is highly influenced by slurry concentration, speed, and pipe diameter. While conveying speed is the main component in the bend section, pipe diameter takes over in the horizontal and vertical pipe sections.

Keywords Coal gangue slurry · Pressure drop · Numerical simulation · Response surface analysis

1 Introduction

Coal gangue, a type of solid waste from coal extraction and processing operations, is typically left on the surface due to its low amount of usable resources (Gao et al. 2021; Xie et al. 2021). However, dispersing poisonous coal gangue in open spaces can cause severe pollution. For instance, when the toxic compounds seep into the earth with rain, they release a significant amount of greenhouse gases and pollute

the groundwater. In addition, fly ash is a byproduct of coal combustion in electric utility plants that are removed from the flue gases using electrostatic precipitators. Every year, the worldwide disposal of fly ash takes up a vast amount of precious land.

Backfill mining is becoming increasingly popular in the mining industry due to its many benefits in lowering pollution. Furthermore, this mining technique is ideal for disposing of the aforementioned solid wastes and reducing the possibility of regional and local ground failure due to collapse or subsidence (Wang et al. 2022a, b; Shi et al. 2021). Because of this, using fly ash and coal gangue instead of traditional Portland cement to make cemented coal gangue paste slurry is of great interest (Senapati and Mishra 2012).

In various industrial sectors, including food production, civil engineering, mining, etc., non-Newtonian slurry must be transported by pipeline to the necessary locations (Kaczmareczyk et al. 2021; Liu et al. 2021). As a result, researchers worldwide undertook extensive research on issues linked to pipeline transportation (Mohsen et al. 2019, 2020; Crawford et al. 2007).

Non-Newtonian fluids have fundamentally different rheological properties than Newtonian fluids, and they are also generally more complex (Picchi et al. 2018, 2017; Chhabra 2010; Sercan and Oney 2020). Therefore, different factors

✉ Qingwen Shi
qs0003@mix.wvu.edu

✉ Helmut Mischo
Helmut.Mischo@mabb.tu-freiberg.de

¹ Department for Underground Mining Methods, Institute of Mining and Special Civil Engineering, Technical University of Bergakademie Freiberg, Fuchsmühlenweg 9, 09599 Freiberg, Dresden, Germany

² Department of Structural Engineering and Building Materials, Faculty of Engineering and Architecture, Ghent University, 9052 Zwijnaarde, Belgium

³ School of Engineering, University of Warwick, Coventry CV47AL, UK

⁴ Department of Engineering, West Virginia University, Morgantown 26505, USA

impact the pressure evolution of non-Newtonian flow in the pipeline. For instance, Qi et al. (2018) created a pilot pipeline system for delivering materials with intricate circuit shapes. The method demonstrated the backfill pressure drop due to the cement paste's reactions to the circuit geometry, inlet pressure, cement-tailing ratio, solid content, and cement content. The authors also examined the relative significance of the factors that affected the pressure drop. According to a study, pressure drop can be considerably impacted by flow velocity, pipe geometry, slurry concentration, and other factors (Haixin 2018). Besides, the cement slurry's physical and chemical characteristics significantly impact pressure drop in a pipe flow (Yang et al. 2020).

Additionally, the study by Easa and Barigon has confirmed the considerable impact that particle size distribution has on flow regime (Easa and Barigou 2009). Similar studies were also conducted by Jiang et al., showing that the particle size and shape can affect the rheological behaviour of the slurry (Jiang et al. 2019). When conveying backfill materials to underground voids through a vertically downward pipeline, Senapati and Mishra advised modifying the diameter and concentration to change the surplus pressure head (Senapati and Mishra 2012). In addition, when estimating pressure drops in the pipeline, some researchers considered chemical reactions; they developed a coupled reaction model and applied it to computational fluid dynamics software. The outcomes demonstrated the impact of the hydration process on the paste flow characteristics (Lang et al. 2019).

Although many researchers have undertaken extensive research on the flow of non-Newtonian fluids through pipes under either single or multiple causes, as noted in the initial introduction, they viewed the pipeline as a whole system. They thus disregarded the flow patterns in various pipe sections. The calculated and actual values of the pipe pressure drop will differ significantly due to the neglect. Additionally, it could jeopardize the material transmission's ability to operate safely or reduce the effectiveness of the pressure pump. As Wu et al. (2015a, b) noted in one of their studies, it is crucial to precisely predict the pressure drop along the pipeline since it will result in a significant energy waste if the pump's pumping capacity is greater than what is needed to convey slurry. In contrast, pipe obstruction will happen when the pump capacity is inadequate (Wu et al. 2015a, b).

Many researchers around the world typically took the traditional approach of running experiments in the lab to evaluate the pressure loss of slurry flow for backfilling through a pipeline (Bharathan et al. 2019; Chandel et al. 2009; Chen et al. 2015). The expensive equipment and the time required for the experimental method substantially deter researchers' excitement, although laboratory experiments can recreate many application scenarios to produce reliable data. More and more researchers have demonstrated that using fluid computing software to simulate the flow of

highly concentrated slurries in pipes is an efficient substitute for conventional lab tests, thanks to the advancements in simulation software and increased computing power (Chen et al. 2017; Wu et al. 2018; Lahiri and Ghanta 2010; Swamy et al. 2015; Kiran et al. 2019). Numerical simulations maximize the replication of field circumstances that cannot be achieved in the laboratory, minimize the expense of experimental materials and equipment, and reduce preparation time (Cayeux and Leulseged 2020; Gao et al. 2020).

A recently developed backfill technology is cementing coal gangue. Compared to the collapse method, this excavation technique offers numerous benefits, including giving workers a secure workspace, preventing surface subsidence, and disposing of underground solid waste (Chen et al. 2020; Liang and Fall 2016). In addition, the flow characteristics of the high-density slurry are compatible with non-Newtonian fluids, remarkably Herschel-Bulkley fluid (Gharib et al. 2016; Mehta et al. 2021). In several studies, the Herschel-Bulkley model is more effective and precise at predicting the rheological properties of non-Newtonian flows (Gharib et al. 2016; Bharathan et al. 2019; Huang et al. 2019; Taibi and Messelmi 2018). Therefore, in the current work, many rheological experiments of the coal-gangue-fly-ash slurry were firstly carried out to gather all the essential data for the subsequent simulation to ascertain how the various elements affect the pressure profile at a different segment of the pipeline. The Herschel-Bulkley model was then used to simulate the impact of the pressure drop's three primary influencing parameters (i.e., flow velocity, pipe diameter, and slurry concentration). Then, pressure drop single-factor analysis and multi-factor response surface analysis were provided.

2 Materials and experiment

2.1 Materials

In Jining, Shandong Province, China, a coal mine crushing plant provided the coal gangue for this study. Some studies suggest that a specific proportion of fine particles in the mixture can help the slurries in the backfill pipeline to transmit steadily and smoothly. Therefore, two steps of coal gangue crushing were performed beforehand to suit the transporting needs. Figure 1 shows the coal gangue's particle size distribution following crushing and more than 70% of the coal gangue particles are less than 5 mm.

The fly ash used in this investigation came from a coal-fired power station in Jining, China, and Fig. 2 shows the particle size distribution. X-ray diffraction analysis of the coal gangue and fly ash's chemical composition resulted in a summary in Table 1. On a Bruker D8 Advance diffractometer, utilizing a step scan mode with a step of 0.075° (2θ) and 4 s per step, X-ray diffraction measurements were carried

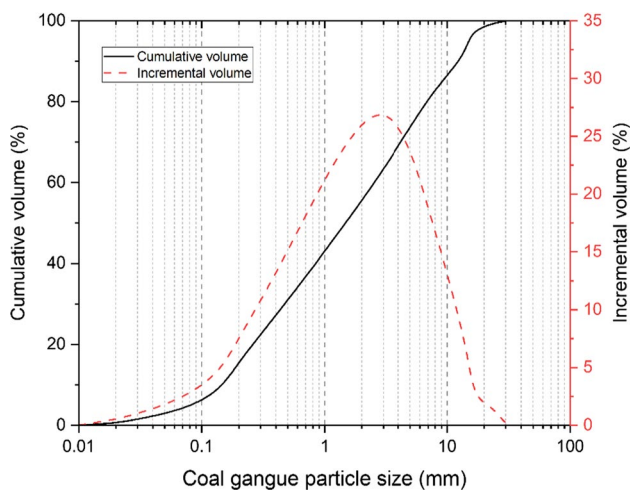


Fig. 1 Coal gangue particle size distribution

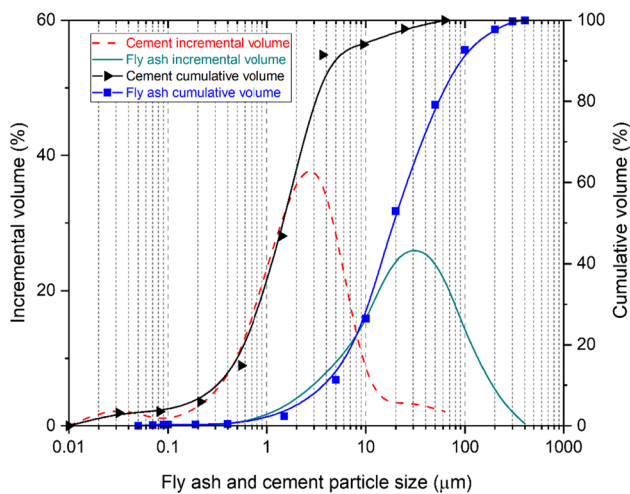


Fig. 2 Fly ash and cement particle size distribution

out. A diffracted beam monochromator and Cu-K α radiation at 35 kV and 30 mA were used to operate the diffractometer in reflection mode. The coal gangue's high SiO₂ content suggests that the backfill mass supporting the nearby rock and layer can fulfil the necessary conditions. Therefore, fly ash is classified as a type C due to its CaO level.

In the present study, 20 wt% fly ash and 80 wt% ordinary Portland cement (Jiang et al. 2020; Wang et al. 2022a, b) are mixed as the binding agent in the backfill slurry. The crushed coal gangue particles are used as aggregates, and

three levels of solid concentration slurry (76 wt%, 77 wt%, and 78 wt%, respectively) were prepared according to the research protocols. The mixing water is municipal tap water.

2.2 Rheological test

A series of rheological tests were carried out in the lab to acquire the essential parameters for the subsequent simulation experiments. First, all mixtures were prepared in proportion, placed in a blender, and stirred for 1 min at a low speed of 100 r/min, then a two-minute 150 r/min stir followed, producing a homogeneous filled slurry. After that, the rheological properties of the slurry samples are assessed using a vane rheometer. The slurry sample was pre-sheared for 30 s at 0.1/s, and then after a 30 s break, the shear rate increased from 0 to 120/s within 90 s to minimize the effects of transferring forces. All rheological information was then recorded using the rheometer's software. The temperature was controlled at 24 ± 1 °C during the test's execution. The shear rate-shear stress relationship of the three slurries with various solid concentrations is depicted in Fig. 3. The connection is not linear, unlike the Newtonian flow, and the yield stress is needed to make the slurry flow. Consequently, based on the rheological experiments and previous scholars' reports, the Herschel-Bulkley model was adopted in this paper (Wang et al. 2022a, b).

3 Model building

This paper developed a three-dimensional model consisting of three components (vertical section, bend section, horizontal section) with the aid of Model-designer software (see Fig. 4). The bend has a radius of 0.5 m and a length of 10 m for both the vertical and horizontal parts. This simulation model was built on the cartesian coordinate system, and six observation planes at $y=0.5$ m, $y=4.0$ m, $y=5.0$ m, $x=0.5$ m, $x=7.0$ m, and $x=8.0$ m, respectively, were set up. In the subsequent data analysis, the pressure difference between the observation planes $y=4.0$ m and $y=5.0$ m represents the mean pressure loss of the slurry at the vertical pipe section. Similarly, the pressure gap between the observation surfaces $y=0.5$ m, and $x=0.5$ m represents the pressure drop at the bend. Finally, the pressure disparity between the observation planes $x=7.0$ m and $x=8.0$ m indicates the average pressure drop at the horizontal stage.

Table 1 Composition of coal gangue and fly ash (%)

Classification	Loss	SiO ₂	Fe ₂ O ₃	Al ₂ O ₃	CaO	MgO	TiO ₂	Na ₂ O	K ₂ O
Gangue	17.8	51.92	3.87	19.03	1.0	1.18	0.75	0.54	1.47
Cement	1.5	21.25	1.85	4.12	65.13	1.58	0.11	0.16	0.70
Fly ash	10.33	43.84	27.40	4.01	12.13	1.09	–	–	–

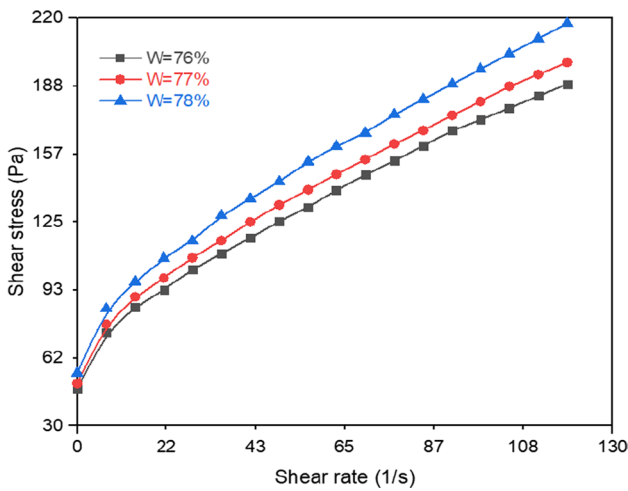


Fig. 3 Backfill slurry rheological property

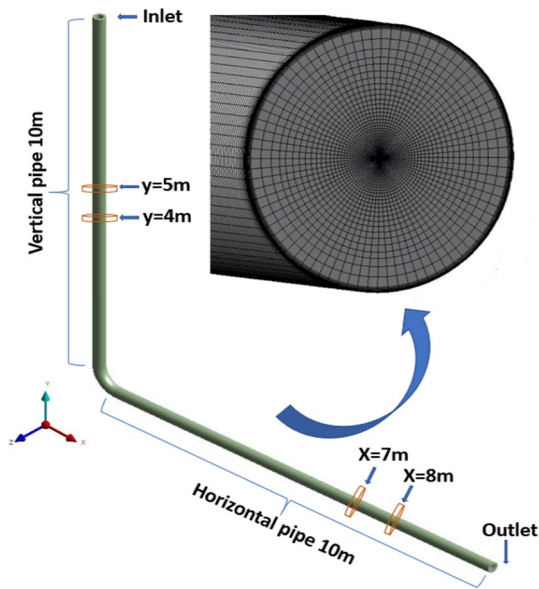


Fig. 4 Mesh of the fluid domain

The Eulerian and Lagrangian methods are the two general approaches used to examine the fluid flow properties. The Lagrangian follows a single fluid parcel as it moves through space and time. In contrast, the Eulerian concentrates on particular locations in the area through which the fluid flows as time passes. Despite the opposing observation direction, there are no significant differences between the two approaches, and the analytical outcomes are the same for the identical problem.

The hexahedral mesh was used due to its good performance in quick convergence and time savings. Furthermore, the boundary layer's inflation function was used to capture the flow characteristics close to the pipe wall (see Fig. 4).

And to confirm the grid's independence, we evaluated six meshes with various mesh densities. The mesh independence tests show that when the mesh is denser than 374,907, a stable MAPE less than 5% is reached which indicates an excellent mesh (Sercan and Oney 2020). In this situation, to balance the simulation accuracy and computational efficiency, we use a mesh of 374,907 elements in the present simulation.

Due to the homogeneous continuous medium characteristics of the filling slurry, both Eulerian and Lagrangian methods are applicable in reconstructing the flow characteristics of the fluid domain. In the present paper, the Eulerian approach was adopted.

The following assumptions are made for the backfill slurry to save computational resources and simplify the numerical model:

- (1) The slurry flow in the pipe is continuous and smoothly;
- (2) The mechanical properties of the slurry are uniform in all directions, resulting in a homogeneous flow;
- (3) The slurry is incompressible, and there is no heat exchange with the external environment during the delivery process.

The governing equations, the mass conservation equation, momentum conservation equation, and energy conservation equation determined the motion of the slurry flow through the pipeline. Solving all of the conservation equations in the fluid domain makes it possible to decide on the slurry's flow characteristics in the pipe. The data can then be analyzed to reveal specific obscure rheological patterns. For example, the symbol for mass conservation is Eq. (1).

$$\frac{\partial \rho}{\partial t} + \text{div} \left(\rho, \begin{matrix} \vec{r} \\ v \end{matrix} \right) = 0 \tag{1}$$

where t is time, ρ is the density of the slurry, and v is the flow velocity of the fluid.

Due to the aforementioned incompressible flow assumption, the concentration of the slurry does not vary with time, so Eq. (1) can be rewritten as:

$$\frac{\partial u}{\partial x} + \frac{\partial v}{\partial y} + \frac{\partial w}{\partial z} = 0 \tag{2}$$

where u , v , and w is the velocity vector component in the x , y , and z -direction, respectively.

The slurry momentum conservation equation can be derived using Newton's second law, as shown in Eqs. (3), (4) and (5).

$$\frac{du}{dt} = X - \frac{1}{\rho} \frac{\partial P}{\partial x} + \mu \left(\frac{\partial^2 u}{\partial x^2} + \frac{\partial^2 u}{\partial y^2} + \frac{\partial^2 u}{\partial z^2} \right) \tag{3}$$

$$\frac{dv}{dt} = Y - \frac{1}{\rho} \frac{\partial P}{\partial y} + \mu \left(\frac{\partial^2 v}{\partial x^2} + \frac{\partial^2 v}{\partial y^2} + \frac{\partial^2 v}{\partial z^2} \right) \quad (4)$$

$$\frac{dw}{dt} = Z - \frac{1}{\rho} \frac{\partial P}{\partial z} + \mu \left(\frac{\partial^2 w}{\partial x^2} + \frac{\partial^2 w}{\partial y^2} + \frac{\partial^2 w}{\partial z^2} \right) \quad (5)$$

here, X , Y , and Z represent the surface force of the fluid micro-element in the x , y , and z directions, respectively. P represents the combined force acting on the fluid micro-element, ρ is the slurry density, and μ denotes the viscosity of the tested slurry. The meaning of other symbols is the same as that of Eq. (2).

The slurry flow in the pipe follows the law of energy conservation and assumes that there is no heat exchange with the external environment. Hence, the Bernoulli equation for the fluid can be written in the following form:

$$z_1 + \frac{P_1}{\gamma} + \frac{V_1^2}{2g} = z_2 + \frac{P_2}{\gamma} + \frac{V_2^2}{2g} + H \quad (6)$$

here, Z_1 and Z_2 represent the spatial position of the fluid micro-element in the pipe, respectively, while P_1 and P_2 are the pressure corresponding to the Z_1 and Z_2 positions. V_1 and V_2 are the flow velocity at positions Z_1 and Z_2 . γ is the bulk density, and H delegates the work done by the pipe friction force on the slurry when it flows from position Z_1 – Z_2 .

The computational fluid program ANSYS was used to run 48 simulations with three primary elements and three levels to thoroughly study the impact of factors on pressure drop along the pipeline and how each aspect impacts pressure drop in the slurry transport process. Table 2 displays the investigational portfolio that was involved.

An appropriate discretization is a foundation for the subsequent simulation. Therefore, it is vital to have a fine mesh for the targeted computational domain, especially for the region with a complex shape (in the present bend section).

Table 2 Model setting

Concentration (wt%)	Velocity (m/s)	Diameter (m)
76	1.5	0.12
	2.0	0.15
	2.5	0.18
	3.0	0.21
	3.0	0.21
77	1.5	
	2.0	
	2.5	
	3.0	
78	1.5	
	2.0	
	2.5	
	3.0	

Therefore, a finer mesh was deployed in the bend to capture the features of slurry flowing through the turn.

The boundary condition for the inlet was velocity inlet with four levels. In addition, the outlet was set to be a pressure outlet with zero static pressure, and the gravity force aligned in the opposite direction of the Y coordinate axis.

4 Results and discussion

4.1 Single factor analysis

4.1.1 Influence of flow velocity on pressure drop

It can be seen from Fig. 5 that the pressure drop of all the investigated concentration-diameter-position combinations increases gradually concerning the increasing slurry velocity when the pipe diameter is 0.15 m. However, the increased speed of the pressure drop varies for each variety. For instance, the growth rate of the pressure-drop of the combination W77D15B, where the two digits after W indicate the percentage of the concentration, the two digits after D indicate the diameter of the pipe in centimetres, the last letter indicates the different pipe parts, in which V represents the vertical part, H means the horizontal portion and B represents the bent pipe part, decreases with the velocity. However, for slurries W76D15H, W76D15V and W76D15B, the opposite behaviour is observed.

Additionally, this diagram shows another distinctive feature: different parts of the pipe exhibit additional pressure losses under the influence of flow velocity. For example, when the solid concentration is 77 wt%, pressure drops much more at the bend section of the pipe than in the corresponding vertical or horizontal area for all velocities. The other

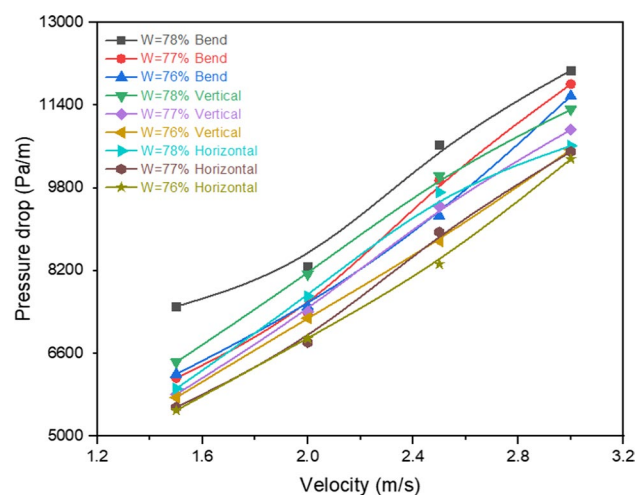


Fig. 5 Pressure drop gradient with velocity when diameter equals 0.15 m

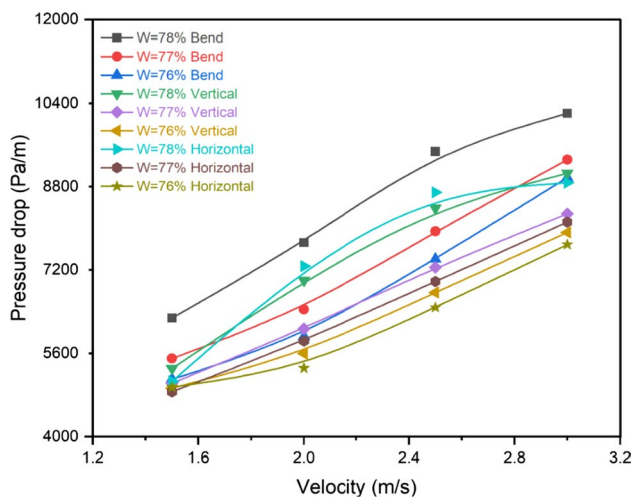


Fig. 6 Pressure drop gradient with velocity when diameter equals 0.18 m

two groups (76 wt% concentration group and 78 wt% concentration group) also showed the same characteristics. The descending order of pressure drop within each concentration group is bend section, vertical section, and horizontal section.

Figure 6 depicts the pressure drop gradient of the slurries with flow velocity when the pipe diameter is 0.18 m. This graph shows that pressure loss increases with increasing speed in all investigated combinations, except for W78D18B and W78D18H. In the case of W78D18B, as the flow rate increases, the increase in pressure loss is gradually slowing down. While for the slurry combination W78D18H, the pressure loss per meter remains almost constant when the flow velocity exceeds 2.5 m/s. Compared to Fig. 5, the most significant difference in Fig. 6 is that the slurry with 78 wt% solid particles consumes more pressure in the horizontal section than the vertical section as the slurry flows below 2.5 m/s.

Figure 7 illustrates how pressure changes along with varying flow velocity in a pipe with a 0.21 m diameter. This chart demonstrates a vast difference compared to the slurry flows in a 0.18 m diameter pipe (see Fig. 6) or a 0.15 m diameter pipe (see Fig. 5). The pressure drop gradient in the bend section of the slurry with 78 wt% concentration is not the largest among all the investigated slurry combinations. At a flow velocity of 3 m/s, the pressure drop gradient in the bend section of W78D21B is less than that of the corresponding slurries W77D21B and W76D21B. In addition, at a flow velocity of 1.5 m/s, the pressure drop value of W78D21B drops to the lowest among all the investigated combinations, indicating that this combination is optimal for energy efficiency under these working conditions. The pressure drop of the slurry in the 78 wt% concentration group generally remains

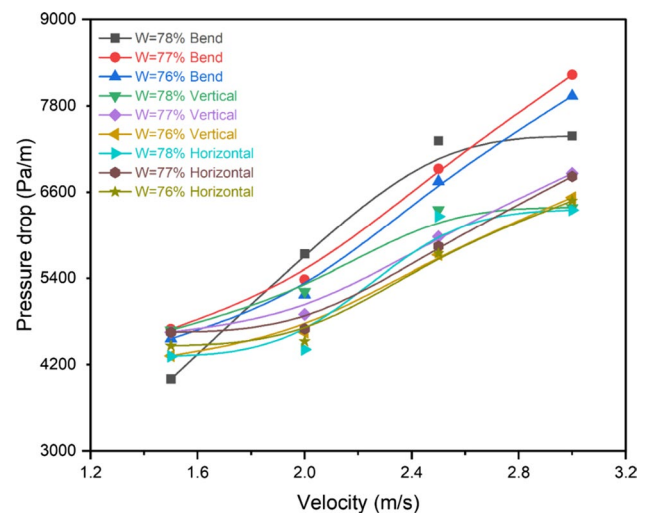


Fig. 7 Pressure drop gradient with velocity when diameter equals 0.21 m

stable when the flow velocity exceeds 2.5 m/s. At the same time, the pressure drop of the 77 wt% and 76 wt% concentration group experiences a steady increase.

The above phenomena show that velocity is not the only factor affecting pressure drop and that velocity acts differently in different parts (bend, vertical and horizontal section) of the pipe.

When the slurry 76 wt% flows at speeds more than 1.8 m/s, the pressure drop almost increases linearly with an increasing velocity at all the pipe sections (namely bend, vertical and horizontal). In contrast, the pressure drop of the slurry with a concentration of 78 wt% grows progressively slower at the bend section of the pipe. It reflects that when slurry flows velocity increases, its influence on pressure loss declines compared with the slurries in 77 wt% and 76 wt% concentration. The pressure loss disparity between slurries with a concentration of 78 wt%, 77 wt%, and 76 wt% is depicted in Figs. 6 and 7. Those two charts demonstrate that the higher the slurry concentration is, the more significant the pressure drop. In addition to the slurry concentration, the flow velocity considerably influences the pressure drop disparities among different test groups.

The gap in pressure drop between the two groups of slurries with a solid concentration of 78 wt% and 77 wt% is most significant at a flow velocity of 2.5 m/s in all pipe sections. In contrast, the minimum pressure drop gap occurs when the flow velocity is 1.5 m/s (see Fig. 6).

However, the changing tendency of the pressure drop gap between slurries of 77 wt% solid concentration and 76 wt% solid concentration appears remarkably different. When the flow speed rises from 2 to 2.5 m/s, the pressure drop gap almost remains stable, regardless of the pipe

section. The pressure drop disparity decreases sharply as the flow velocity increases from 2.5 to 3 m/s (see Fig. 7).

4.1.2 Influence of solid concentration on pressure drop

Slurry concentration is a decisive consideration in the slurry preparation (Gao et al. 2020; Wu et al. 2015a, b; Li et al. 2019) and it dominates the strength development of the backfill mass. This section focuses on the effect of slurry concentration on pressure drop in different pipe sections.

Figure 8 exhibits the effect of different slurry concentrations on the pressure drop of the slurry flowing through other parts of the pipe with a 0.18 m diameter. All the curves in the graph show that the pressure drop increases with increasing concentration and accelerates at concentrations above 77 wt%. The pressure disparities between different concentration groups at a separate pipe section were depicted in Figs. 9 and 10. It clearly illustrates that the change of slurry concentration has an evident influence on the pressure drop and the scale of this influence depends on which part of the pipe the slurry is flowing by. For example, when the flow velocity is 2 m/s, the pressure drop gap between slurries with a concentration of 78 wt% and 77 wt% at the horizontal section is the largest. On the other hand, the slightest pressure drop gap appears at the vertical section of the pipe. At a flow velocity of 3 m/s, the difference in pressure drop in the bend section is slightly greater than in the horizontal and vertical areas (see Fig. 8).

When the flow velocity is below 2.5 m/s, the change tendency of the pressure drop disparity between slurries with the concentration of 77 wt% and 76 wt% is similar to that of slurries with a concentration of 78 wt% and 77 wt%, except the corresponding pressure drop gaps are somewhat narrower (see Figs. 8 and 9). However, as shown in Fig. 9, when

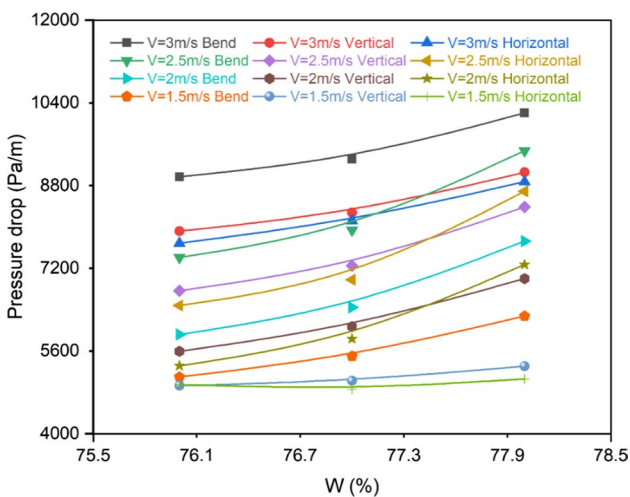


Fig. 8 Pressure drop gradient with concentration when diameter equals 0.18 m

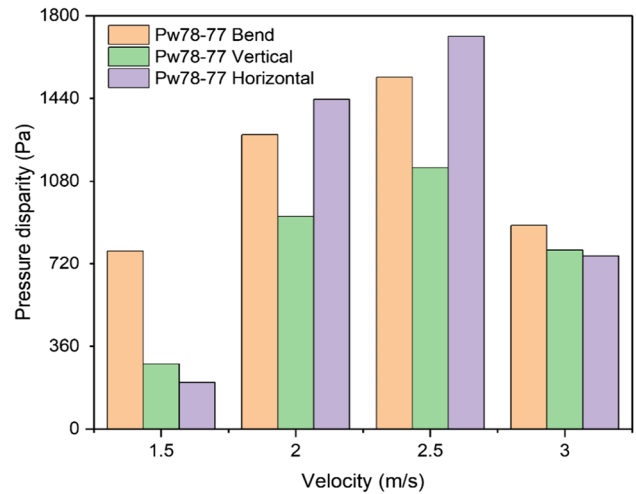


Fig. 9 Pressure drop disparity between slurry Pw78 and Pw77 when the diameter is 0.18 m

the flow velocity reaches 1.5 m/s, the pressure drop difference between slurry in concentration 78 wt% and slurry in concentration 77 wt% at the horizontal section becomes the least significant. The histogram in Fig. 10 depicts a point utterly different from the others, i.e. a negative value. This point presents that when a more concentrated slurry flows through the horizontal pipe section, it loses less energy than a less concentrated slurry.

The gradually increasing tendency of pressure-drop with a rising velocity of the slurries for all investigated groups is generally similar when the pipe diameter is 0.18 m, except that the pressure drop's growth speed varies from each other. For instance, when the solid concentration is 76 wt%, the pressure drop increases almost linearly with an increasing velocity at all the pipe sections (namely bend, vertical and

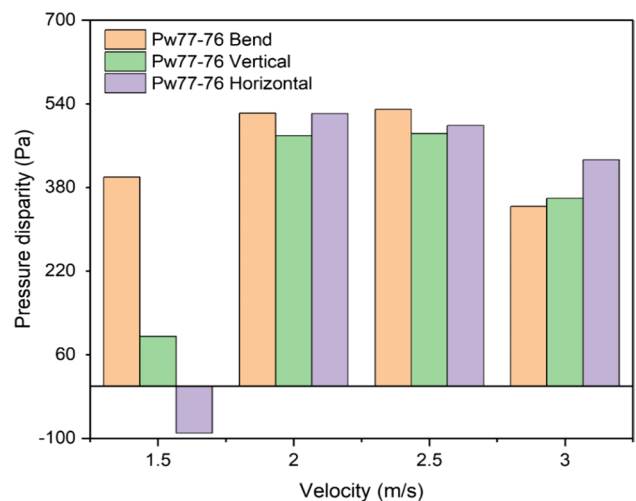


Fig. 10 Pressure drop disparity between slurry Pw77 and Pw76 when the diameter is 0.18 m

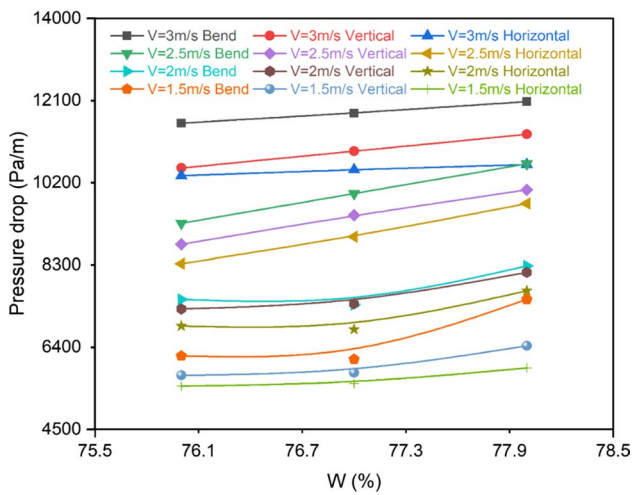


Fig. 11 Pressure drop gradient with concentration when diameter equals 0.15 m

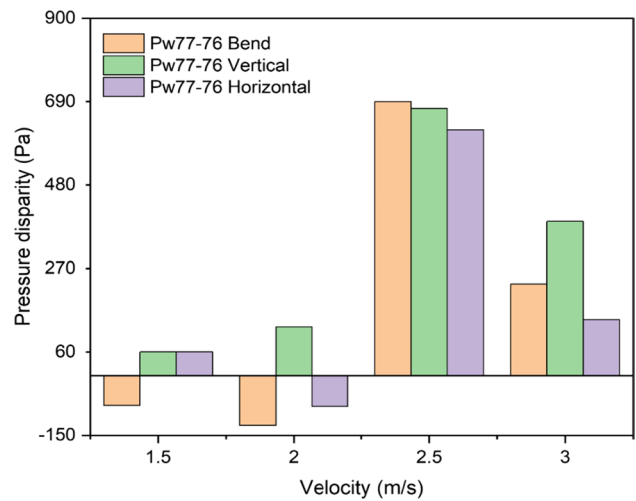


Fig. 13 Pressure drop disparity between slurry Pw77 and Pw76 when the diameter is 0.15 m

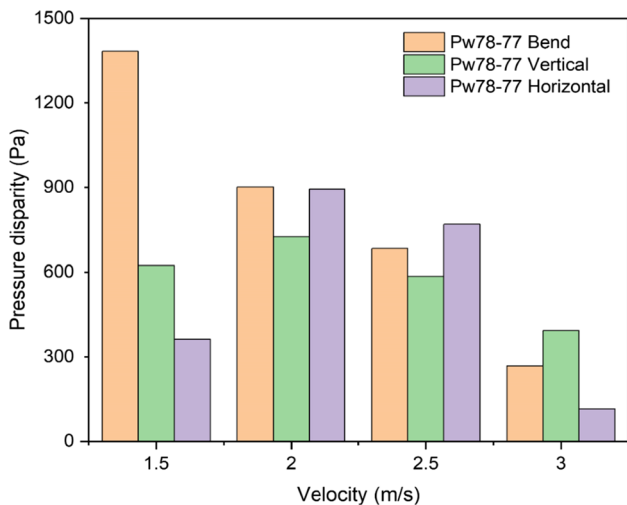


Fig. 12 Pressure drop disparity between slurry Pw78 and Pw77 when the diameter is 0.15 m

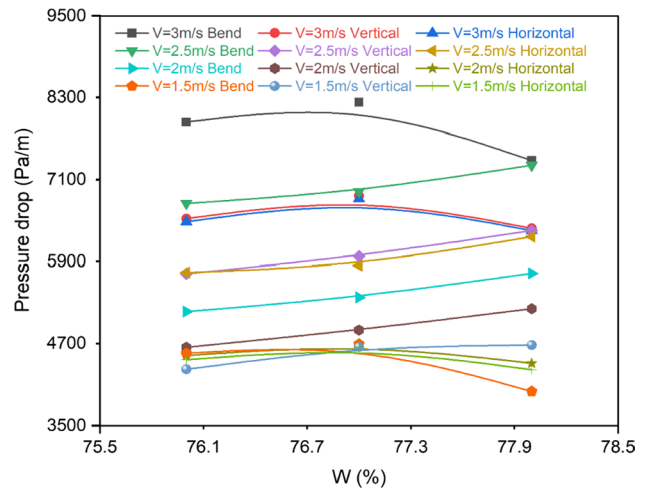


Fig. 14 Pressure drop gradient with concentration when diameter equals 0.21 m

horizontal). However, at the bend section of the pipe, the pressure drop shows a more significant rise than the vertical and horizontal parts.

As shown in Fig. 11, most of the investigated slurry combinations follow the pattern of increasing pressure drop with growing concentration except for slurry W77D15B and W77D15H. This unusual variation is illustrated more clearly in Figs. 12 and 13. The pressure drop disparities in all sections of the pipeline are all positive, indicating that the 78 wt% concentration slurry indeed loses more pressure than the 77 wt% concentration slurry, despite the different pressure drop gaps in the corresponding sections of the pipeline (see Fig. 12). However, when the slurry flows 2 m/s in the bend and horizontal area of the pipe, the slurry

with a concentration of 77 wt% has less pressure reduction than the slurry with 76 wt% (see Fig. 13). The reason behind this anomaly is likely to be the superimposition of expected effects of pipe diameter, slurry velocity, and concentration.

If comparing Fig. 14 with Figs. 11 and 8, it is easy to notice that as the concentration rises, the pressure loss of the slurry in the larger diameter pipes is substantially different from that in, the smaller diameter pipes. For example, the pressure drop of all the slurry combinations as the solid concentration increases from 76 wt% to 77 wt%. However, when the concentrate continues to grow to 78 wt%, some varieties of pressure drop are reduced conversely (see Fig. 14).

Figure 15 reflects the gap of pressure drop between slurries with the concentration of 77 wt% and 78 wt%. When the

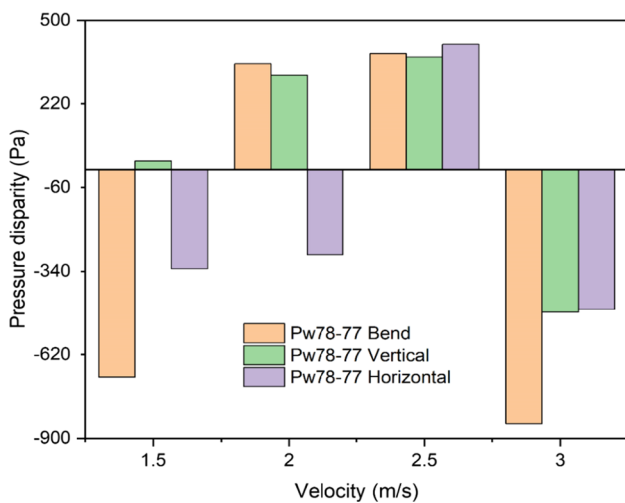


Fig. 15 Pressure drop disparity between slurry Pw78 and Pw77 when the diameter is 0.21 m

velocity is 3 m/s, the slurry with 78 wt% concentration loses less pressure than the slurry with 77 wt% concentration, both in the vertical and horizontal sections and bend sections. In the horizontal section, the slurry with 78 wt% concentration also consumes less pressure than the slurry with 77 wt% concentration when the velocity is 2 m/s and 1.5 m/s. This negative pressure drop may be that the diameter of the pipe plays a dominant role in such conditions compared to the concentration and rate.

The positive values shown in Fig. 16 indicate that more energy is required to provide sufficient pressure to transport a high concentration slurry than a low concentration slurry. The phenomenon is consistent with what is demonstrated in Fig. 14.

4.1.3 Influence of pipe diameter on pressure drop

Figures 17, 18 and 19 reproduced how the pressure drops with changing pipe diameter. It is evident from these three charts that the increasing pipe diameter will facilitate the reduction of pressure loss and thus save energy needed for transportation. The 76 wt% concentrate slurry and 77 wt% concentrate slurry groups showed a strong regularity. In the same velocity subgroups, the pressure drop of the bend section is always the highest while the horizontal section is the lowest (Figs. 17 and 18). However, it becomes more complex in terms of the 78 wt% concentration slurry group. A comparison with Figs. 17 and 18 reveals that the most obvious difference is that all the curves in Fig. 19 are convex in shape. That implies that when the slurry concentration is 78 wt%, the pressure drop decreases gently in the lower diameter range. On the other hand, the pressure drop reveals a relatively sharp decline in the higher diameter range. Therefore, 0.18 m is the inflexion point of pipe diameter,

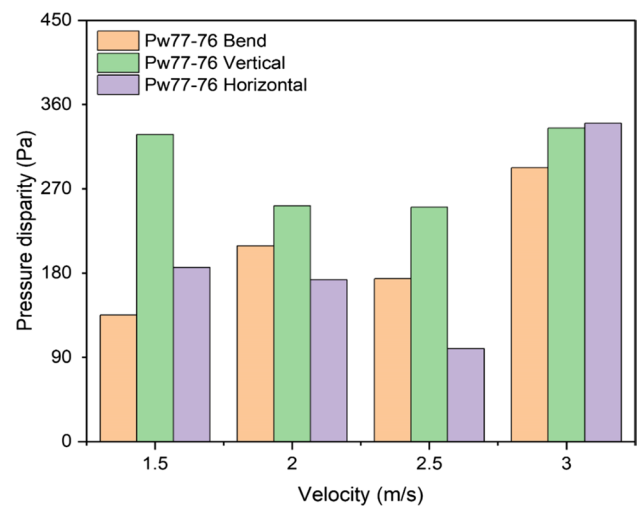


Fig. 16 Pressure drop disparity between slurry Pw77 and Pw76 when the diameter is 0.21 m

which deserves special attention when designing the pipeline system for conveying slurries.

4.2 Multi-factor response surface analysis

The above analysis clarifies that pressure drop is the combined result of many different factors. Thus, we must carefully study each component to comprehend the law of pressure loss. However, considering every element would be unreasonable or expensive, certain implications are only modest in specific circumstances and can be temporarily overlooked. Therefore, the weights of slurry concentration, flow rate, and pipe diameter on pressure losses in various

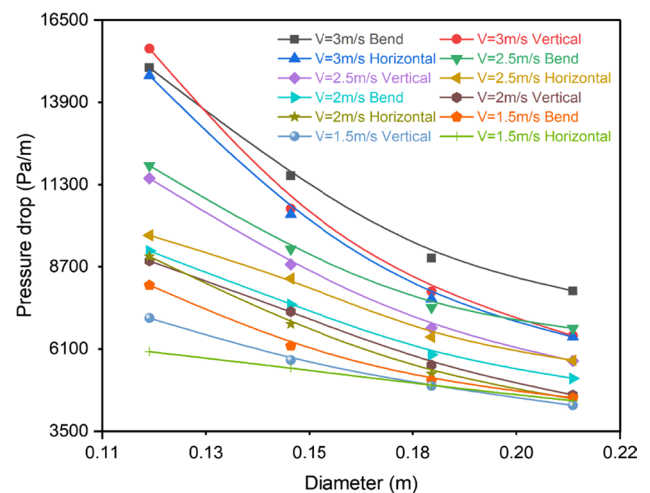


Fig. 17 Pressure drop gradient with diameter when concentrate equals 76%

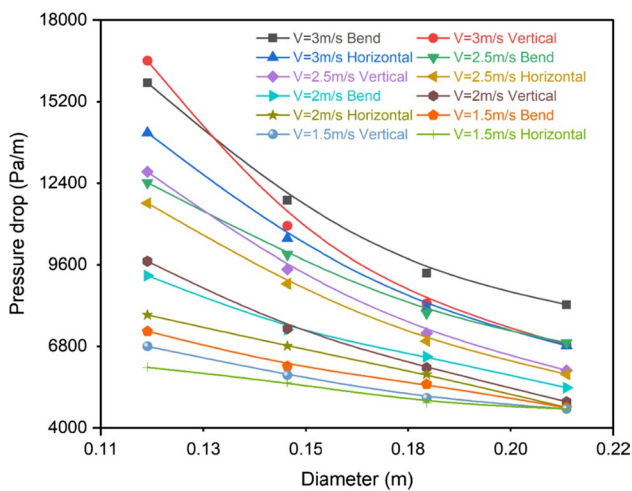


Fig. 18 Pressure drop gradient with diameter when concentrate equals 77%

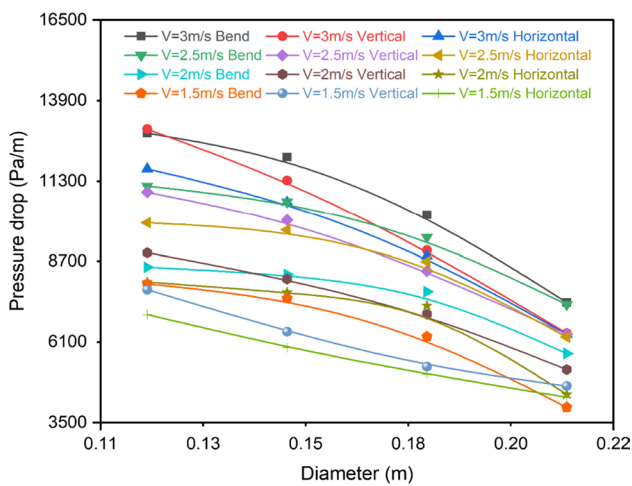


Fig. 19 Pressure drop gradient with diameter when concentrate equals 78%

pipe sections were calculated using the response surface approach and the software Design expert (Stat-Ease Inc.).

Response surface methodology (Yusri et al. 2018) is a collection of mathematical and statistical techniques that can analyze all the dominant factors and influence the dependent variable (Kazeem et al. 2018). A

central composite design with three independent variables (namely the pipe diameter, slurry velocity, and concentration) at three levels was performed by applying the Design Expert 12. After 144 runs in total, the fit summary of different fitting models' accuracy and practicality at the bend section, vertical section, and horizontal section are listed in Tables 3, 4 and 5. From which, the most suitable model was automatically presented. As for the bend and vertical parts of the pipe, the 2FI model is suggested, while the linear model is recommended for the horizontal section. Given that the 2FI model is inferior to the linear model only in the Predicted R^2 and the consistency with the vertical and bend section, all the following analyses were based on the 2FI model. Finally, the general form of the 2FI model is demonstrated as Eq. (7).

$$Y = B_0 + \sum_{i=1}^n B_i X_i + \sum_{i=1}^{n-1} \sum_{j=i+1}^n B_{ij} X_i X_j + \epsilon \tag{7}$$

where Y is the dependent response, B_0 is the constant coefficient, B_i is the linear coefficient and B_{ij} is the interaction coefficient, n is the number of factors investigated in the present paper, while the term X_i and $X_i X_j$ are the independent variables and the interactions, respectively. The ϵ represents the random error.

4.2.1 Response surface analysis at a vertical section

Table 6 shows that the Model F -value is 42.25, which implies that the model is significant in the vertical section. There is only a 0.01% chance that this large F -value could occur due to noise. P -values less than 0.05 indicate model terms are significant. In this case, velocity, diameter, and concentration are important model terms. P -values greater than 0.1 indicate the model terms are not practical. Hence, the velocity-diameter combination term significantly influences the pressure drop more than the other two combination terms.

The R square indicates that 98% of the variation in the pressure drop depends on the independent variable. In comparison, the coefficient of variation of 3.9% explains a high degree of accuracy.

The coefficients of all the independent variables are presented in Table 7. The weights of each independent variable

Table 3 Comparison of different models at bend section

Source	Sequential P -value	Adjusted R^2	Predicted R^2	Remarks
Linear	<0.0001	0.9117	0.8567	
2FI	0.0332	0.9432	0.8657	Suggested
Quadratic	0.3479	0.9461	0.7673	
Cubic	0.0074	0.9886	-3.4145	Aliased

Table 4 Comparison of different models in vertical section

Source	Sequential <i>P</i> -value	Adjusted <i>R</i> ²	Predicted <i>R</i> ²	Remarks
Linear	< 0.0001	0.9330	0.8856	
2FI	0.0064	0.9670	0.9209	Suggested
Quadratic	0.1265	0.9752	0.8891	
Cubic	0.0097	0.9942	- 1.2409	Aliased

Table 5 Comparison of different models in the horizontal section

Source	Sequential <i>P</i> -value	Adjusted <i>R</i> ²	Predicted <i>R</i> ²	Remarks
Linear	< 0.0001	0.9153	0.8740	Suggested
2FI	0.1933	0.9265	0.8407	
Quadratic	0.5673	0.9213	0.6889	
Cubic	0.0119	0.9803	- 6.6249	Aliased

Table 6 Analysis of variance for response surface model at vertical section

Source	Sum of squares	df	Mean square	<i>F</i> -value	<i>P</i> -value
Model	3.748×10^7	6	6.247×10^6	42.25	< 0.0001
A-velocity	1.217×10^7	1	1.217×10^7	82.31	< 0.0001
B-diameter	2.213×10^7	1	2.213×10^7	149.69	< 0.0001
C-concentration	2.452×10^6	1	2.452×10^6	16.58	0.0022
AB	6.079×10^5	1	6.079×10^5	4.11	0.0701
AC	17755.56	1	17755.56	0.1201	0.7361
BC	99698.06	1	99698.06	0.6743	0.4307

Note: C.V. = 3.9% *R*-Squared = 0.98 Adj *R*-Squared = 0.97 Predicted *R*-Squared = 0.92

on the response variable were determined based on the estimated coefficient value. In the vertical part of the pipe, the most influential factor in reducing slurry pressure is the diameter of the pipe, followed by the conveying speed of the slurry. The minor significant factor among those three independent factors is the concentration of the slurry. Although pipe diameter is negatively related to pressure drop, the effect of pipe size on pressure loss is consistent with that

described in Sect. 4.1.3. Regarding the interaction term, the AB has a more significant influence on the pressure drop than AC (velocity and concentration) and BC (diameter and concentration).

The three-dimensional response surface was plotted to reveal better the interactions of the three operating variables and how they contribute to the pressure drop during slurry conveying. Two independent variables were analyzed in each case during the investigation, while the other variable was kept constant (see Fig. 20). From Fig. 20a, it can be seen that the value of pressure-drop experienced a pronounced increase when the pipe diameter decreased from 0.21 to 0.12 m, and the flow velocity increased from 1.5 to 3.0 m/s at the same time. If the diameter is constant, the pressure losses will increase rapidly with the continuous increase in slurry concentration and flow velocity. However, as Fig. 20c illustrates, under the precondition that the flow speed remains constant, an increase in slurry concentration and a decrease in pipe diameter can lead to a sharp rise in pressure loss. Another interesting phenomenon that the Fig. 20c shows is that for all the combinations of concentration and pipe diameter investigated, the maximum pressure loss does not occur at the combination with the smallest pipe diameter and the highest concentration. This not only confirms the

Table 7 Coefficients of coded factors in vertical section

Factor	Coefficient estimate	df	Standard error	95% CI low	95% CI high	VIF
Intercept	7526.21	1	93.26	7318.41	7734.01	
A-velocity	1233.42	1	135.95	930.50	1536.35	1.0000
B-diameter	- 1663.37	1	135.95	- 1966.30	- 1360.45	1.0000
C-concentration	553.58	1	135.95	250.65	856.50	1.0000
AB	- 389.83	1	192.27	- 818.22	38.57	1.0000
AC	- 66.62	1	192.27	- 495.02	361.77	1.0000
BC	- 157.88	1	192.27	- 586.27	270.52	1.0000

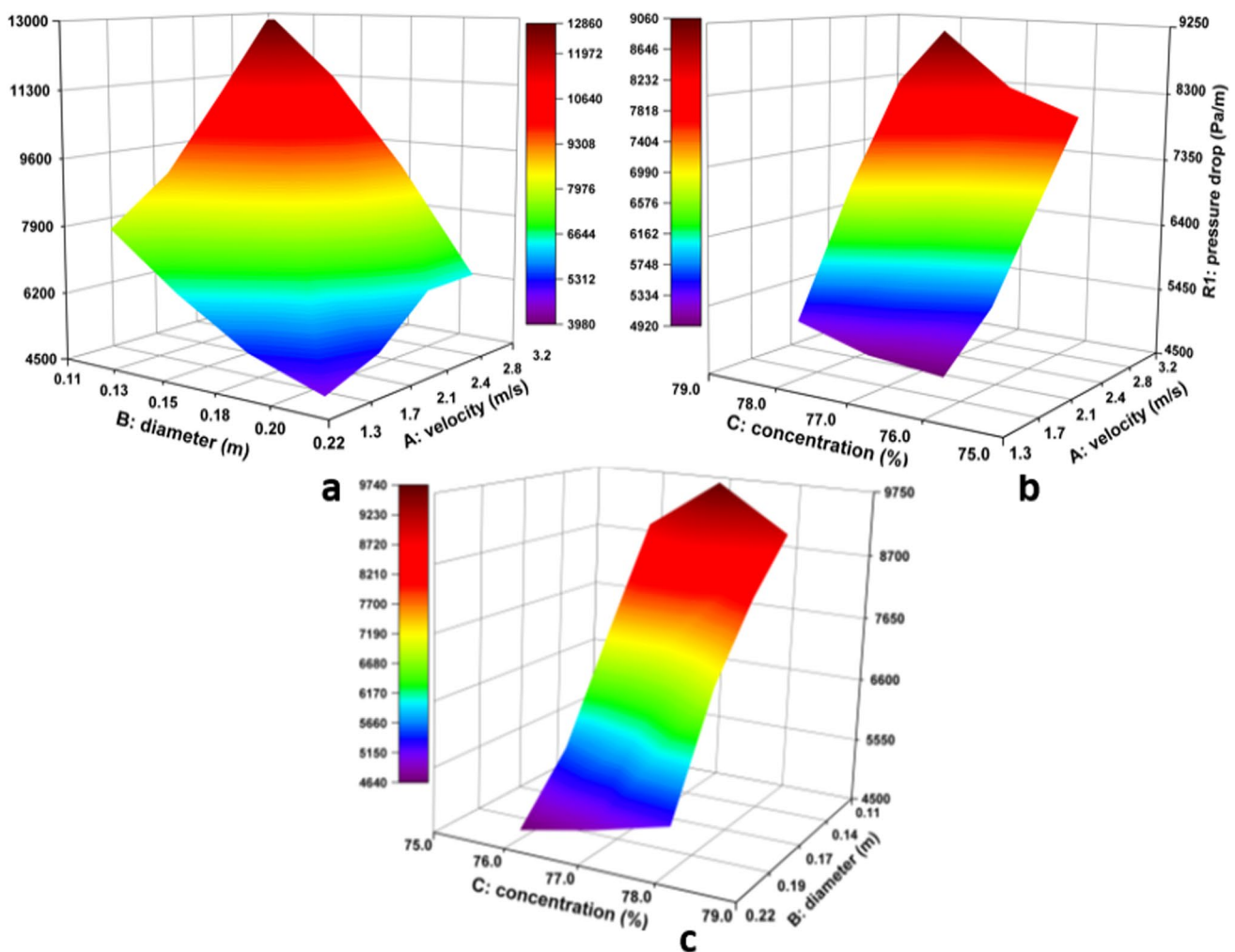


Fig. 20 Response surface at vertical section

synchronicity between slurry concentration and pipe diameter in influencing the pressure loss, but also suggests that the 77% concentration is a possible special concentration that needs to be investigated in a more detailed way.

4.2.2 Response surface analysis at bend section

According to the *P*-value, the outstanding practicality of the 2FI model is confirmed at the pipe bends. In addition, all the three investigated dependent variables (namely velocity, diameter, and concentration) significantly influence the responding pressure drop, and the interaction term AB has a considerable impact as well (see Table 8). From Table 9, the weights of each independent variable and combination term on the effect of pressure drop can be derived from the estimated coefficient. Unlike in vertical pipes, velocity is the most critical factor affecting the pressure in the bend section. On the other hand, slurry concentration followed the pipe diameter and ranked the third independent variable

Table 8 Analysis of variance for response surface model at bend section

Source	Sum of squares	df	Mean square	<i>F</i> -value	<i>P</i> -value
Model	4.075×10^7	6	6.791×10^6	56.19	<0.0001
A-velocity	2.052×10^7	1	2.052×10^7	169.76	<0.0001
B-diameter	1.627×10^7	1	1.627×10^7	134.65	<0.0001
C-concentration	3.091×10^6	1	3.091×10^6	25.57	0.0005
AB	6.207×10^5	1	6.207×10^5	5.14	0.0469
AC	81827.46	1	81827.46	0.6771	0.4298
BC	1.648×10^5	1	1.648×10^5	1.36	0.2700

Note: C.V. = 4.96% *R*-Squared = 0.96 Adj *R*-Squared = 0.94 Predicted *R*-Squared = 0.87

in determining pressure drop, although pipe diameter and pressure drop are negatively correlated.

Table 9 Coefficients of coded factors at bend section

Factor	Coefficient estimate	df	Standard error	95% CI low	95% CI high	VIF
Intercept	8193.75	1	84.32	8005.89	8381.62	
A-velocity	1601.43	1	122.91	1327.57	1875.29	1.0000
B-diameter	-1426.22	1	122.91	-1700.09	-1152.36	1.0000
C-concentration	621.55	1	122.91	347.68	895.41	1.0000
AB	-393.92	1	173.82	-781.21	-6.62	1.0000
AC	-143.03	1	173.82	-530.32	244.27	1.0000
BC	-202.99	1	173.82	-590.29	184.30	1.0000

Figure 21 shows the effect of pipe diameter, slurry concentration, and flow velocity on pressure drop at the bend section. However, its tendency to vary with the combination of pipe diameter and velocity is not constant, and combinations scattered in different ranges show significant differences in their contribution to the degree of pressure loss. The combination of pipe diameter and velocity (0.15 m, 2.4 m/s) appears to be a watershed in the trend of

pressure loss variation, with combinations distributed on either side of this combination demonstrating an abrupt change in the effect on pressure loss (Fig. 21a). As shown in Fig. 21b, flow velocity and slurry concentration worked together to control the tendency for pressure variation. When the slurry concentration was low, there was a relatively significant increase in pressure loss with an equivalent rise in flow velocity. Although the corresponding

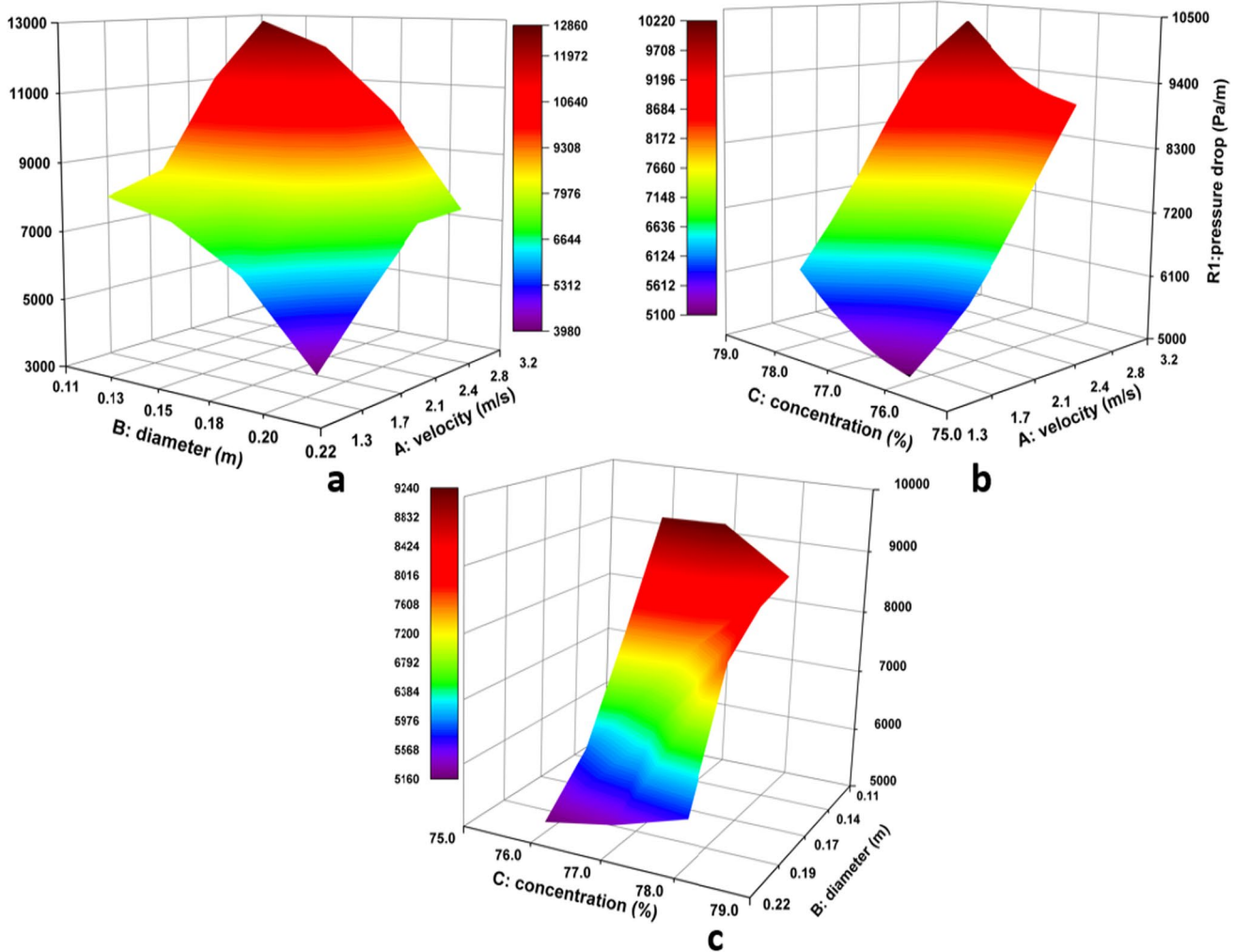


Fig. 21 Response surface at bend section

value is different, Fig. 21c shows a similar response surface to Fig. 20c.

4.2.3 Response surface analysis at the horizontal section

The *R*-square and adjusted *R*-square have proved the accuracy of the 2FI model in analyzing the pressure drop dataset. The *P*-values in Table 10 show that flow velocity, pipe diameter, and slurry concentration can remarkably influence the pressure loss of slurry flowing through the horizontal section of the conveying pipe.

The value of the coefficient estimate in Table 11 shows that the pipe diameter is the independent variable with the most significant influence on pressure drop. On the other hand, the AC (velocity and concentration) interaction term is the least influencing independent factor.

Figure 22 reveals the three-dimensional response surface of pressure drop at the horizontal section of the pipe. The general changing tendency of the pressure drop under the action of all the three independent variables is similar to the corresponding one in vertical section of the pipe except the response surface of pressure loss to concentration and diameter. In the response surface Fig. 22c, the slurry concentration shows a different effect on the pressure loss, i.e. when the pipe diameter is kept constant, the response surface forms a clearly visible groove at the concentration of

77%. The special profile of the response surface shows that any combination of pipe diameter and slurry concentration can save transport energy at a slurry concentration of 77%, which not only further confirms the outstanding performance of the response surface method in the qualitative analysis of multifactor coupling, but also provides a realistic reference for the selection of the filling slurry concentration.

5 Conclusions

Numerous factors affect the pressure loss when conveying slurry through a pipeline and the three most crucial factors are the pipeline's diameter, the slurry's concentration, and the flow rate. In this paper experimental tests, numerical simulations and response surface methods were employed to analyse how the above factors alone affect pressure loss during pipeline transport and how multiple factors jointly affect pressure reduction. The results show that the main factors influencing pressure loss are not invariable, for example a dominant factor can become secondary due to changes in pipe geometry, and the same factor can have different effects on pressure loss due to a combination with different influencing factors. The following are some specific findings:

- (1) The shear rate- shear stress tests of the filling slurries prepared in the present research reveal that the Herschel-Bulkley model can capture the slurry's rheological characteristics better and is therefore recommended when numerical simulation need to be implemented.
- (2) Compared to the slurry flowing through the vertical and horizontal pipe sections, the slurry flowing through the bends exhibits the largest pressure loss and consequently the most severe pipe wear due to the dramatic change in flow pattern. Hence, it is advisable to present special treatment on the bent part for a more scientific pipe network design.
- (3) The response surface method was used to statistically analyse the values of the pressure loss at each section of the pipeline and the factors causing the difference in pressure loss, and the results showed that the flow velocity is the dominant factor in the bend section,

Table 10 Analysis of variance for response surface model at the horizontal section

Source	Sum of Squares	df	Mean Square	<i>F</i> -value	<i>P</i> -value
Model	3.365×10^7	6	5.608×10^6	11.90	0.0005
A-velocity	1.197×10^7	1	1.197×10^7	25.41	0.0005
B-diameter	1.753×10^7	1	1.753×10^7	37.21	0.0001
C-concentration	3.190×10^6	1	3.190×10^6	6.77	0.0264
AB	6.135×10^5	1	6.135×10^5	1.30	0.2804
AC	1.480×10^5	1	1.480×10^5	0.3142	0.5875
BC	1.895×10^5	1	1.895×10^5	0.4021	0.5402

Note: C.V. = 6.07% *R*-Squared = 0.95 Adj *R*-Squared = 0.93 Predicted *R*-Squared = 0.84

Table 11 Coefficients of coded factors in the horizontal section

Factor	Coefficient estimate	df	Standard error	95% CI low	95% CI high	VIF
Intercept	7432.39	1	166.49	7061.43	7803.34	
A-velocity	1223.36	1	242.69	682.61	1764.12	1.0000
B-diameter	-1480.49	1	242.69	-2021.25	-939.73	1.0000
C-concentration	631.48	1	242.69	90.72	1172.23	1.0000
AB	-391.63	1	343.22	-1156.38	373.12	1.0000
AC	-192.38	1	343.22	-957.13	572.36	1.0000
BC	-217.64	1	343.22	-982.38	547.11	1.0000

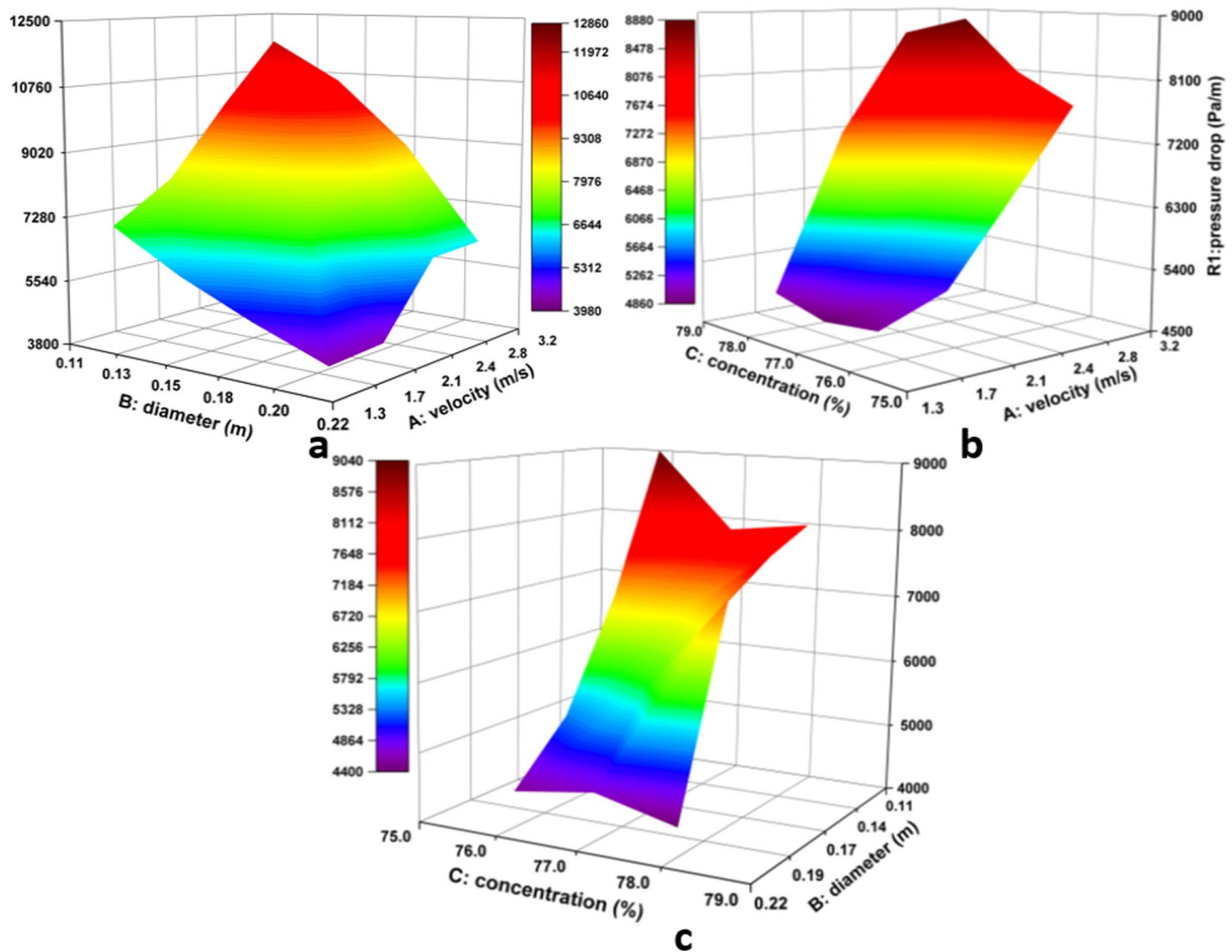


Fig. 22 Response surface at the horizontal section

while in the vertical and horizontal areas, pipe diameter plays a role in determining the pressure loss.

- (4) The efficiency of the response surface method in demonstrating the influence of the independent variable on the dependent variable in a vivid three-dimensional diagram and screening out the major and minor factors utilizing mathematical-statistical analysis proves its potential to be a practical tool in pipeline design.

Acknowledgements The first author would like to thanks the China Scholarship Council for their support.

Funding The authors did not receive support from any organization for the submitted work.

Data availability The data used to support the findings of this study are available from the first author upon request.

Declarations

Conflict of interest The authors declare no conflict of interest in connection with the work submitted.

Open Access This article is licensed under a Creative Commons Attribution 4.0 International License, which permits use, sharing, adaptation, distribution and reproduction in any medium or format, as long as you give appropriate credit to the original author(s) and the source, provide a link to the Creative Commons licence, and indicate if changes were made. The images or other third party material in this article are included in the article's Creative Commons licence, unless indicated otherwise in a credit line to the material. If material is not included in the article's Creative Commons licence and your intended use is not permitted by statutory regulation or exceeds the permitted use, you will need to obtain permission directly from the copyright holder. To view a copy of this licence, visit <http://creativecommons.org/licenses/by/4.0/>.

References

- Bharathan B, McGuinness M, Kuhar S, Kermani M, Hassani FP, Sasmito AP (2019) Pressure loss and friction factor in non-Newtonian mine paste backfill: modelling, loop test and mine field data. *Powder Technol* 344(15):443–453. <https://doi.org/10.1016/j.powtec.2018.12.029>
- Cayeux E, Leulseged A (2020) The effect of thixotropy on pressure losses in a pipe. *Energies* 6165(13):1–23. <https://doi.org/10.3390/en13236165>
- Chandel S, Seshadri V, Singh SN (2009) Effect of additive on pressure drop and rheological characteristics of fly ash slurry at high concentration. *Part Sci Technol* 27(3):271–284. <https://doi.org/10.1080/02726350902922036>
- Chen J, Chen Q, Zhang Q, Li H (2015) Computer simulation of filling slurry pipeline transportation using fluent. *Sci Technol Rev* 33(9):64–68. <https://doi.org/10.3981/j.issn.1000-7857.2015.09.011>
- Chen X, Zhou J, Chen Q, Shi X, Gou Y (2017) CFD simulation of pipeline transport properties of mine tailings three-phase foam slurry backfill. *Minerals* 7(149):1–19. <https://doi.org/10.3390/min7080149>
- Chen S, Du Z, Zhang Z, Yin D, Feng F, Ma J (2020) Effects of red mud additions on gangue-cemented paste backfill properties. *Powder Technol* 367:833–840. <https://doi.org/10.1016/j.powtec.2020.03.055>
- Chhabra RP (2010) Non-newtonian fluids: an introduction. In: Krishnan J, Deshpande A, Kumar P (eds) *Rheology of complex fluids*. Springer, New York, NY
- Crawford NM, Cunningham G, Spence SWT (2007) An experimental investigation into the pressure drop for turbulent flow in 90° elbow bends. *Proc Inst Mech Eng Part E J Process Mech Eng* 221(2):77–88. <https://doi.org/10.1243/0954408jpm84>
- Eesa M, Barigou M (2009) CFD investigation of the pipe transport of coarse solids in laminar power law fluids. *Chem Eng Sci* 64(2):322–333. <https://doi.org/10.1016/j.ces.2008.10.004>
- Gao X, Li T, Rogers WA, Smith K, Gaston K, Wiggins G, Parks JE II (2020) Validation and application of a multiphase CFD model for hydrodynamics, temperature field and RTD simulation in a pilot scale biomass pyrolysis vapor phase upgrading reactor. *Chem Eng J*. <https://doi.org/10.1016/j.cej.2020.124279>
- Gao S, Zhao G, Guo L, Zhou L, Yuan K (2021) Utilization of coal gangue as coarse aggregates in structural concrete. *Constr Build Mater* 268:121212. <https://doi.org/10.1016/j.conbuildmat.2020.121212>
- Gharib N, Bharathan B, Amiri L, McGuinness M, Hassani FP, Sasmito AP (2016) Flow characteristics and wear prediction of Herschel-Bulkley non-Newtonian paste backfill in pipe elbows. *Can J Chem Eng* 95(6):1181–1191. <https://doi.org/10.1002/cjce.22749>
- Haixin Z (2018) Study on the rheological properties and pressure loss of filling slurry with unclassified tailings in pipeline. Master's thesis, North China University of Science and Technology, pp 30–36
- Huang Y, Zheng W, Zhang D, Xi Y (2019) A modified Herschel-Bulkley model for rheological properties with temperature response characteristics of polysulfonated drilling fluid. *Energy Sour Part A Recovery Utilization Environ Effects* 42(12):1464–1475. <https://doi.org/10.1080/15567036.2019.1604861>
- Jiang G, Wu A, Wang Y, Li J (2019) The rheological behavior of paste prepared from hemihydrate phosphogypsum and tailing. *Constr Build Mater* 229:1–9. <https://doi.org/10.1016/j.conbuildmat.2019.116870>
- Jiang H, Fall M, Yilmaz E, Li Y, Yang L (2020) Effect of mineral admixtures on flow properties of fresh cemented paste backfill: assessment of time dependency and thixotropy. *Power Technol* 372:258–266
- Kaczmarczyk K, Kruk J, Ptaszek P, Ptaszek A (2021) Pressure drop method as a useful tool for detecting rheological properties of non-Newtonian fluids during flow. *Appl Sci* 2021(11):6583. <https://doi.org/10.3390/app11146583>
- Kazeem KS, Akeem OA, Mohammed DA (2018) Application of response surface methodology for the modelling and optimization of sand minimum transport condition in pipeline multiphase flow. *Pet Coal* 60(2):339–348
- Kiran R, Ahmed R, Shlehi S (2019) Experiments and CFD modelling for two phase flow in a vertical annulus. *Chem Eng Res Des* 153:201–211. <https://doi.org/10.1016/j.cherd.2019.10.012>
- Lahiri S, Ghanta KC (2010) Regime identification of slurry transport in pipelines: a novel modelling approach using ANN & differential evolution. *Chem Ind Chem Eng Q* 16(4):329–343. <https://doi.org/10.2298/CICEQ091030034L>
- Lang L, Zhiyu F, Chongchong Q, Bo Z, Lijie G, Song KI-IL (2019) Numerical study on the pipe flow characteristics of the cemented paste backfill slurry considering hydration effects. *Powder Technol* 343:454–464. <https://doi.org/10.1016/j.powtec.2018.11.070>
- Li X, Zhou Y, Zhu Q, Zhou S, Min C, Shi Y (2019) Slurry preparation effects on the cemented phosphogypsum backfill through an orthogonal experiment. *Minerals* 9:31. <https://doi.org/10.3390/min9010031>
- Liang C, Fall M (2016) Mechanical and thermal properties of cemented tailings materials at early ages: influence of initial temperature, curing stress and drainage conditions. *Constr Build Mater* 125:553–563
- Liu G, Gong W, Wu H, Lin A (2021) Experimental and CFD analysis on the pressure ratio and entropy increment in a cover-plate pre-swirl system of gas turbine engine. *Eng Appl Comput Fluid Mech* 15(1):476–489. <https://doi.org/10.1080/19942060.2021.1884600>
- Mehta D, Krishnan A, Radhakrishnan T, Von Lier JB, Clemens FHLR (2021) Assessment of numerical methods for estimating the wall shear stress in turbulent Herschel-Bulkley slurries in circular pipes. *J Hydraul Res* 59(2):196–213. <https://doi.org/10.1080/00221686.2020.1744751>
- Mohsen B, Oscar ECH, Vicente SFM, Maria TV, Helena MR (2019) Computational fluid dynamics for sub-atmospheric pressure analysis in pipe drainage. *J Hydraul Res*. <https://doi.org/10.1080/00221686.2019.1625819>
- Mohsen A, Alireza R, Pedram T (2020) Numerical analysis of fluid hammer in helical pipes considering non-Newtonian fluids. *International J Press Vessels Piping* 181:104068. <https://doi.org/10.1016/j.ijpvp.2020.104068>
- Picchi D, Poesio P, Ullmann A, Brauner N (2017) Characteristics of stratified flows of Newtonian/non-Newtonian shear-thinning fluids. *Int J Multiph Flow*. <https://doi.org/10.1016/j.ijmultiphaseflow.2017.06.005>
- Picchi D, Ullmann A, Brauner N (2018) Modeling of core-annular and plug flows of Newtonian/non-Newtonian shear-thinning fluids in pipes and capillary tubes. *Int J Multiph Flow* 103(1):43–60. <https://doi.org/10.1016/j.ijmultiphaseflow.2018.01.023>
- Qi C, Chen Q, Fourie A, Zhao J, Zhang Q (2018) Pressure drop in pipe flow of cemented paste backfill: experimental and modeling study. *Powder Technol Vol* 333(15):9–18. <https://doi.org/10.1016/j.powtec.2018.03.070>
- Senapati PK, Mishra BK (2012) Design considerations for hydraulic backfilling with coal combustion products (CCPs) at high solids concentrations. *Powder Technol* 229:119–125. <https://doi.org/10.1016/j.powtec.2012.06.018>
- Sercan G, Oney E (2020) Eric van oort frictional pressure losses of non-Newtonian fluids in helical pipes: applications for atomized rheology measurements. *J Nat Gas Sci Eng* 73:1–16. <https://doi.org/10.1016/j.jngse.2019.103042>

- Shi Q, Xu G, Wang D et al (2021) Chain pillar optimization at a long-wall coal mine based on field monitoring results and numerical model analysis. *Arab J Geosci* 14:2537. <https://doi.org/10.1007/s12517-021-08843-0>
- Stat-Ease Inc. <https://www.statease.com/software/design-expert/>
- Swamy M, Gonzalez DN, Twerda A (2015) Numerical modelling of the slurry flow in pipelines and prediction of flow regimes. *WIT Trans Eng Sci* 89(2015):311–322. <https://doi.org/10.2495/MPF150271>
- Taibi H, Messelmi F (2018) Effect of yield stress on the behavior of rigid zones during the laminar flow of Herschel-Bulkley fluid. *Alex Eng J* 57(2):1109–1115. <https://doi.org/10.1016/j.aej.2017.01.001>
- Wang D, Barakos G, Cheng Z, Mischo H, Zhao J (2022a) Numerical simulation of pressure profile of mining backfill fly-ash slurry in an L-shaped pipe using a validated Herschel-Bulkley model. *J Sustain Cement Based Mater*. <https://doi.org/10.1080/21650373.2021.2012723>
- Wang D, Cheng Z, Shi Q et al (2022b) Simulation study of velocity profile and deflection rate of non-Newtonian fluids in the bent part of the pipe. *Geofluid*. <https://doi.org/10.1155/2022/7885556>
- Wu D, Yang B, Liu Y (2015a) Pressure drop in loop pipe flow of fresh cemented coal gangue–fly ash slurry: experiment and simulation. *Adv Powder Technol* 26(3):920–927. <https://doi.org/10.1016/j.apt.2015.03.009>
- Wu D, Yang B, Liu Y (2015b) Transportability and pressure drop of fresh cemented coal gangue-fly ash backfill (CGFB) slurry in pipe loop. *Powder Technol*. <https://doi.org/10.1016/j.powtec.2015.06.072>
- Wu A, Yang Y, Cheng H-Y, Chen S-M, Han Y (2018) Status and prospects of paste technology in China. *Chinese J Eng* 40(5):518–525. <https://doi.org/10.13374/j.issn2095-9389.2018.05.001>
- Xie Y, Chi X, Li H, Wang F, Yan L, Zhang B, Zhang Q (2021) Coal and gangue recognition method based on local texture classification network for robot picking. *Appl Sci* 11(23):11495. <https://doi.org/10.3390/app112311495>
- Yang X, Xiao B, Gao Q, He J (2020) Determining the pressure drop of cemented Gobi sand and tailings paste backfill in a pipe flow. *Constr Build Mater* 255:119371. <https://doi.org/10.1016/j.conbuilmat.2020.119371>
- Yusri IM, Abdul Majeed APP, Mamat R, Ghazali MF, Awad OI, Azmi WH (2018) A review on the application of response surface method and artificial neural network in engine performance and exhaust emissions characteristics in alternative fuel. *Renew Sustain Energy Rev* 90:665–686. <https://doi.org/10.1016/j.rser.2018.03.095>

Publisher's Note Springer Nature remains neutral with regard to jurisdictional claims in published maps and institutional affiliations.